Dual Drug Loaded Nanotheranostic Platforms as a Novel Synergistic Approach to Improve Pancreatic Cancer Treatment

Particle
& Particle Systems Characterization
www.particle-journal.com

Dual Drug Loaded Nanotheranostic Platforms as a Novel Synergistic Approach to Improve Pancreatic Cancer Treatment

*Sugata Barui, Marzia Conte, Nicolò Maria Percivalle, Rocío María García Montero, Luisa Racca, Marco Allione, and Valentina Cauda**

This study focuses on the development of theranostic, dual drug-loaded nanocarriers to propose a proof-of-principle therapeutic approach in the treatment of pancreatic ductal adenocarcinoma (PDAC). The nanoconstructs consist of a core of zinc oxide nanocrystals doped with gadolinium, useful as a potential contrast agent in magnetic resonance imaging applications. After functionalizing their surface with amino-propyl groups, the physical adsorption of two hydrophobic drugs is performed: Vismodegib and Sorafenib. Their synergistic use might improve PDAC treatment and stroma depletion when co-delivered in the tumor microenvironment for future in vivo applications. To enhance the nanoconstructs' biostability, the ensemble is coated by a lipid bilayer and a tumor targeting peptide is incorporated on the outer shell surface. As a first proof of concept, the resulting nanoconstructs are tested against two pancreatic cancer cell lines, showing a modest increase in treatment efficacy compared to the free drug counterparts and proving to spare healthy pancreatic cells. In a second testing set, the dual-drug loaded nanoconstructs are tested on both cell lines previously sensitized to a first-line chemotherapeutic drug, Gemcitabine, showing an improved treatment response. From these preliminary results, the nanotheranostic platforms might constitute a good starting point for future PDAC therapy and diagnosis studies.

1. Introduction

Pancreatic ductal adenocarcinoma (PDAC) remains one of the most lethal human malignancies having an overall 5-years survival rate less than 10%.[1] According to a recent update from the International Agency for Research on Cancer, 495'773 new cases were diagnosed with pancreatic cancer in 2020 worldwide and the related death were 466'003 (with an incidence of 4.7% with respect to all diagnosed tumors).[2] Abundant fibrotic stroma and poor vascularization are the typical features of PDAC, limiting the delivery of chemotherapeutics to the tumor site.[3–5] Therefore, the development of novel therapeutic systems able to specifically target tumor stroma as well as neoplastic cells while enabling treatment monitoring is a particularly desirable goal in treating this malignancy.[6,7]

Paracrine hedgehog (HH) signaling from pancreatic cancer cells to stromal cells has been identified as an important promoter of stromal desmoplasia,[8,9] and the inhibition of HH signaling pathway has been the object of many therapies aimed at depleting tumor stroma.[10,11] However, the administration of a HH pathway inhibitor can increase vascularity, which in turn may provoke an enhanced tumor aggressiveness. Moreover, the clinical limitations of this approach have been partly explained by the recently discovered dual role of tumor stroma, which is now well-known to both support and restrain PDAC.[12] On the other side, vascular endothelial growth factor (VEGF) is a potent pro-angiogenic factor, whose overexpression occurs in >90% of PDAC, promoting tumor growth, invasion, and metastases.[13] Thus, VEGF signaling represents an attractive anti-angiogenic therapeutic target in human PDAC.[14] Nonetheless, the anti-angiogenic therapy in PDAC is poorly effective because drug delivery is impaired by high interstitial pressures and collapsed vessels.[15] Motivated by this challenge, we hypothesize that it might be possible to improve the efficacy of anti-angiogenic therapy if the vascular endothelial growth factor receptor (VEGFR) kinase inhibitor was administered simultaneously with a stromal depleting agent known to increase perfusion and vascular promotion. This approach is referred to as tumor microenvironment normalization,[16] and it has been shown to be a preferable treatment with respect to complete vascular and stromal depletion.[17]

Although the combination of HH pathway inhibitor and VEGFR kinase inhibitor here proposed possess considerable potential, the limited targeted delivery, low drug bioavailability,

S. Barui, M. Conte, N. M. Percivalle, R. M. G. Montero, L. Racca, M. Allione, V. Cauda
Department of Applied Science and Technology
Politecnico di Torino
Corso Duca degli Abruzzi 24, Turin 10129, Italy
E-mail: valentina.cauda@polito.it

The ORCID identification number(s) for the author(s) of this article can be found under https://doi.org/10.1002/ppsc.202200138.

DOI: 10.1002/ppsc.202200138

and high hydrophobicity of the two drugs in question could reduce their effectiveness. For these reasons, we propose here the use of molecularly targeted and smart drug carriers, already reported in previous literature reviews,[18] to achieve a dual drug codelivery and their consequent synergistic action.

Rapid growth in bionanotechnologies applied to cancer therapy has resulted in the development of various nanomedicine products[19,20] and in the implementation of novel theranostic approaches.[21,22] In particular, nanoparticles (NPs)[19,23–28] and more specifically zinc oxide nanocrystals (ZnO-NCs) have shown great potential application in vitro as well as in vivo for targeted therapy, due to their biocompatibility and pH-sensitivity, that assure effective endosomal drug release.[29–31] Moreover, ZnO-NCs can be probed for magnetic resonance imaging (MRI) when doped with metals or rare earth elements (i.e., gadolinium),[32] which might help the detection of drug-loaded NPs in deep-seated tumors such as pancreatic cancer.[33]

To limit ZnO-NCs aggregation in biological media, reduce their fast dissolution in toxic Zn^{2+} ions and increase their biocompatibility,[34] a phospholipidic coating based on commercially available lipids is here implemented. Actually, the use of ZnO NCs shielded by a lipid bilayer has already been the topic of previously reported studies, which assessed the enhanced biostability of the final nanoconstructs and their effective application in various branches of cancer treatment.[35,36] In contrast, uncoated ZnO NCs can show important cytotoxic effects, due to the dissolution and release of zinc cations (Zn^{2+}) and the reactive oxygen species (ROS) generation, as reported in a recent review on the topic.[30] In this work, due to Sorafenib and Vismodegib poor solubility in aqueous media, their loading is carried out by means of two successive physical adsorptions on the surface of ZnO-NCs in non-polar solvents, whose selection and order are carefully designed and tuned to achieve an optimized process.

The dual drug loaded ZnO nanocrystals here developed are coated with a lipid bilayer by means of the freeze-thaw technique, reported by our group in previous studies[30,37] and active targeting is accomplished by the use of the tumor homing peptide CKAAKN,[39] potentially able to interact with the Wnt-2 pathway, and thus to target both the pancreatic cancer cells and the tumor microenvironment, specifically the angiogenic vessels,[39] in vivo. The resulting nanoconstructs are thoroughly characterized from a physical and chemical point of view, to achieve an optimized nanoplatform. As a first proof of concept, the obtained lipid-coated nanocrystals (LNCs) are tested on different cell lines: Two tumoral, BxPC-3 (a human PDAC cell line derived from pancreas) and AsPC-1, (a human PDAC cell line derived from metastatic site) and a healthy one, HPDE (healthy cells derived from normal human pancreatic duct epithelial). Finally, the nanocarriers are administered to the afore-mentioned cell lines following a Gemcitabine pre-treatment, aimed at obtaining a basic idea of sensitized PDAC cells. The interesting preliminary results obtained so far support the future use of these LNCs as a feasible nanotheranostic tool, thanks to their potential as dual drug nanocarriers. Nevertheless, these data undoubtedly deserve further future research toward 3D models in vitro and in vivo applications to assess the nanoconstructs' synergistic action against PDAC in more accurate biomimetic models.

2. Experimental Section

2.1. Synthesis and Amine-Functionalization of Oleic Acid Stabilized Gadolinium-Doped ZnO Nanocrystals

The synthesis of gadolinium-doped ZnO nanocrystals (Gd-doped ZnO- NCs) was carried out following a rapid wet chemical co-precipitation method, as previously described by some of us.[33] More in details, 0.5268 g of zinc acetate dihydrate (2.4 mmol) and 0.0963 g of gadolinium(III) acetate hydrate were dissolved into 40 mL of absolute ethanol in a round-bottom glass flask. The desired molar ratio of zinc acetate dihydrate and the dopant was 1:0.12. Subsequently, 140 µL of oleic acid was added. The reaction flask was then assembled with a refrigeration column and immersed in a silicon oil heating bath, set to 70 °C, under constant stirring at 350 rpm. After reaching the target temperature, 0.522 g of tetramethylammonium hydroxide, dissolved into 1.052 mL of bidistilled water and then mixed with 10 mL of absolute ethanol, were rapidly added to the reaction mixture. The so-obtained colloidal solution evolved from transparent to white. After 15 min of stirring, the reaction was interrupted by immersing the flask in an ice bath and quickly adding 40 mL of ice-cold (0–4 °C) ethanol. The resulting nanocrystals were collected by centrifugation (at 10 000 RCF for 5 min), the reaction's supernatant was discarded, and the pelleted nanomaterial washed with 30 mL of fresh ethanol, vortexed and sonicated in an ultrasound bath to improve the disaggregation process, and then centrifuged again. The washing process was repeated twice and the resulting Gd-doped oleic capped ZnO NCs were obtained as a colloidal suspension in ethanol. To obtain the NCs concentration, an empty Eppendorf tube was carefully weighed, filled by a known amount of colloidal NC suspension and then dried at RT overnight, to assess the dry weight of the NCs.

A following amino-propyl functionalization step was carried out on the ZnO- NCs surface. A volume of colloidal suspension corresponding to 40 mg of NCs was introduced in a round-bottom flask and diluted with ethanol down to final concentration of 2.5 mg mL^{-1} concentration. The reaction mixture was heated up to 70 °C and refluxed under continuous flow of nitrogen. Afterward, 12.5 µL of (3-aminopropyl)trimethoxysilane (corresponding to 14.6 mol% of the total amount of ZnO- NCs) was added and the reaction was carried out for 6 h. After this time, the reaction mixture was let to cool down and then centrifuged at 10 000 RCF for 10 min. The supernatant was removed, 5 mL of ethanol was added to resuspend the pellet, followed by sonication and vortexing, and two washing steps were performed. The final aminopropyl functionalized, oleic acid-capped, and Gd-doped ZnO NCs were obtained as a colloidal suspension in ethanol (EtOH) of known concentration and kept at room temperature (RT) as stock solution, from which the volume corresponding to a certain weight of NCs was withdrawn each time to perform the experiments.

2.2. Nanocrystals Chemo–Physical Characterization

Field emission scanning electron microscope (FESEM) assisted by energy dispersive spectroscopy (EDS) was performed for

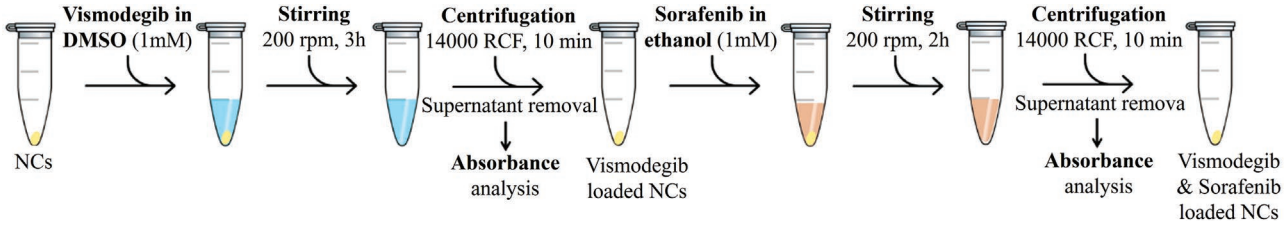

Figure 1. Schematic representation of the optimized dual drug uptake process.

the evaluation of the morphology and elemental analysis of the NCs, using a Merlin microscope from Zeiss (Jena, Germany) with an accelerating voltage of 10 and 15 kV for EDS.

To assess the crystallinity of the obtained NCs, X-ray diffraction (XRD) analyses were performed with a with a Panalytical X'Pert diffractometer in θ–2θ Bragg–Brentano mode (Cu-Kα radiation source, λ = 1.54 Å, 40 kV, and 30 mA). For both FESEM and XRD characterizations, the analyses were performed on dried samples prepared by spotting a certain amount of colloidal solution on a silicon substrate.

Dynamic light scattering (DLS) was employed for the assessment of size distribution and Z-potential of NCs suspensions in ethanol and water (just in water for Z-potential measurements) at a concentration of 100 µg mL^{-1}, with a Zetasizer Nano ZS90 (Malvern Instruments, Worcestershire, UK).

2.3. Drug Uptake

Sorafenib (Sigma-Aldrich) and Vismodegib (AstaTech, Inc.) were purchased from Sigma-Aldrich and AstaTech, respectively. For both drug uptake analyses and drug release experiments, calibration curves were calculated by measuring the absorbance spectrum of each drug in its respective solvent (as justified below, Sorafenib in EtOH, Vismodegib in both EtOH and dimethyl sulfoxide, DMSO) and also in cell culture medium, RPMI (American Type Culture Collection, ATCC) completed with fetal bovine serum (ATCC) at 10%v/v and penicillin-streptomycin at 1% v/v (Sigma-Aldrich) using a UV–vis spectrometer (MultiscanGO, Thermo Scientific). Starting from stock solutions of 5 mM of Sorafenib in ethanol and 10 mM of Vismodegib in DMSO, five solutions were prepared for each drug (0.01, 0.1, 1, 10, 100 and 1000 µM) and analyzed in triplicate using a synthetic quartz glass microplate (96 wells, Hellma Analytics).

For drug adsorption onto the ZnO NCs, two different procedures were carried out: a single drug uptake, performed to tune some important process parameters, and then the dual drug uptake experiment.

For the optimization of the correct drug uptake time, 100 µg of amino-propyl functionalized Gd-doped ZnO NCs were separated by centrifugation (14 000 RCF for 10 min) from ethanol and a 1 mM solution of either Vismodegib in DMSO or Sorafenib in ethanol was added; magnetic stirring was then performed at RT at 200 rpm to allow the drug uptake on the NCs. The drug adsorption on the NCs was then assessed at different time steps (from 1 to 6 h) investigating the UV–vis absorbance of the drug solution before and after uploading; for the background subtraction, the free solvent was used. Briefly, after a specific time step the sample was centrifuged, the NCs pellets separated from the supernatant drug solution and the latter analyzed in triplicate. The amount of adsorbed drug on the NCs surface was determined by the subtraction of the solution concentration to the starting drug solution (1 mM) and applying the calibration curve plotted as described above.

After optimizing the process, as thoroughly described in the Section 3, the dual drug loading on the NCs was finally performed as follows: 100 µg of NCs were collected by centrifugation (14 000 RCF for 10 min) in a 1.5 mL tube and, after EtOH removal, 200 µL of 1 mM Vismodegib in DMSO solution was added. Magnetic stirring was performed at RT for 3.5 h at 200 rpm. The obtained Vismodegib-loaded NCs were then centrifuged (14 000 RCF, 10 min), the supernatant was collected for uptake analyses using UV–vis spectroscopy, and 200 µL of 1 mM Sorafenib in ethanol was added. Magnetic stirring was performed at RT for 2 h at 200 rpm, then the supernatant was collected by centrifugation and analyzed. **Figure 1** reports a scheme of the optimized dual drug uptake protocol described above.

The obtained dual drug-loaded NCs were either used immediately or kept at −20 °C for further preliminary studies, such as lipid coating and cell treatments. In this latter case, all the above-mentioned protocols were conducted under a bio-safety hood, in sterile conditions.

2.4. Nanoconstruct Preparation

Single and dual drug-loaded amino-functionalized oleic-capped Gd-doped ZnO NCs were coated by a lipid bilayer, using liposomes and exploiting a freeze-thaw technique in liquid nitrogen, after having carefully optimized a precise number of freeze-thaw cycles as reported in a recently published work from our group.[38] Two kinds of liposomes were separately prepared using commercially available lipids: DOPC (1,2-dioleoyl-sn-glycero-3-phosphocholine, Avanti Polar Lipids Inc.) liposomes, and a second type composed of DOPC and a functional lipid made by DSPE-PEG(2000)-maleimide (Avanti Polar Lipids Inc.) conjugated to the CKAAKN targeting peptide (custom made from BioFab Lab).

To prepare the DOPC liposomes (hereafter called Lipo), 2.5 mg of DOPC were collected from the stock solution in chloroform, dried in a glass vial, and dispersed in 400 µL of EtOH and 600 µL of water. From this new stock solution (having a concentration of 2.5 mg mL^{-1}), 100 µL was withdrawn, dispersed in 900 µL bidistilled, and 0.1 µm microfiltered water and then sonicated for 5 min to produce a DOPC liposomal solution (0.25 mg mL^{-1}).

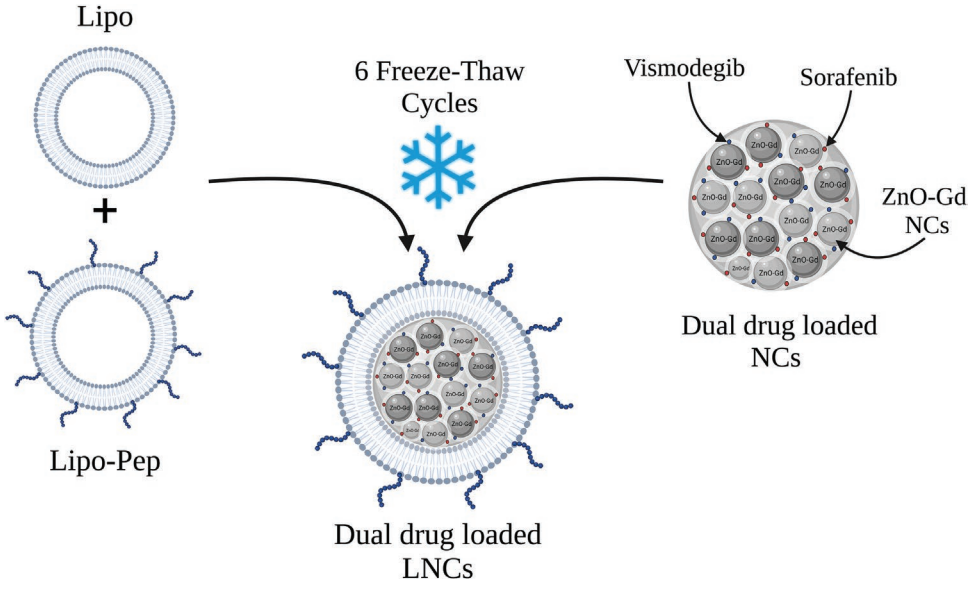

Figure 2. Coupling of DOPC liposome (Lipo) and DOPC:DSPE-PEG-CKAAKN liposome (Lipo-Pep) with dual drug-loaded, amine functionalized, Gd-doped ZnO NCs with freeze-thaw technique to obtain the final nanoconstructs (LNCs). Created with Biorender.com

The target ligand-coupled liposomes (hereafter called Lipo-Pep) was prepared by first conjugating the lipid DSPE-PEG(2000)-maleimide with the cysteine residue of the CKAAKN peptide (as explained in detail in Supporting Information) and then fusing it to a solution of DOPC liposomes.

Finally, both Lipo and Lipo-Pep preparations were separately incubated at 37 °C for 8 h under orbital shaking at 200 rpm. This process aimed at the stabilization of both the so-formed liposomes and, in the case of Lipo-Pep, also at the correct incorporation of the peptide compound into the lipidic shell. Ultimately, both samples were separately dialyzed to allow the removal of the unbound peptide in the Lipo-Pep formulation, and the process was performed also on the Lipo sample to subject it to the same protocol. SnakeSkin Dialysis Tubing (3.5K MWCO, 16 mm dry I.D., 35 feet, Thermofisher Scientific) was used and the dialysis was carried against 1 L of bidistilled water for 18 h under gentle magnetic stirring (70–80 rpm).

The lipid coating of the NCs was performed exploiting a freeze-thaw technique: The desired amount of drug-loaded NCs (and also of unloaded NCs, for control) as pellet was resuspended in a proportion of 1 µL of bidistilled water for each 10 µg of NCs, and vigorously mixed in a cryovial. Then, aliquots of both Lipo and Lipo-Pep solutions were added according to the following ratio: 1:0.5:0.5, where 1 refers to the volume (µL) of Lipo, 0.5 to the volume (µL) of Lipo-Pep, and 0.5 to the weight (µg) of NCs. This ratio is the result of an optimized procedure derived from a long lab experience,[38] which aimed at finding the best compromise between an efficient lipid coating—thus employing an adequate amount of lipids—and a reduced amount of CKAAKN peptide, whose free presence might cause toxicity to cells and would result in a waste of a highly specific and expensive compound. The cryo vial was subject to 6 freeze-thaw cycles, where 1 cycle consisted in freezing the sample solution in the cryovial in liquid nitrogen at –196 °C for 3 min and thawing it at RT for 30 min. After the 6th cycle, the obtained LNCs were stabilized with 1 h of orbital shaking at 200 rpm at 37 °C. The entire process is schematized in **Figure 2**.

To prepare a control sample, the two liposome formulations Lipo and Lipo-Pep were also freeze-thawed using the same process described above, but without including the ZnO NCs. The resulting control sample is hereinafter named Lipo-Lipo-Pep.

2.5. Lipid-Coated Nanocrystals Nanoconstruct Characterization

Optical fluorescence microscopy was performed with a wide-field fluorescence inverted microscope (Nikon Eclipse Ti-E), equipped with a high-resolution camera (Zyla 4.2 Plus, 4098 × 3264 pixels, Andor Technology) using a 60x and a 100x immersion oil objective (Plan Apo 1.40, Nikon), with a super bright wide-spectrum source (Shutter Lambda XL), operating with NIS-element software. To validate the LNCs preparation, liposomes were labelled by exploiting a FITC dye (excitation peak 495 nm, emission peak 519 nm) covalently bound to the CKAAKN peptide, and the related images were obtained in the green channel. Before the freeze-thaw process, the ZnO NCs were conjugated through the amine-functional groups with Atto550 NHS ester (excitation peak 544 nm, emission peak 576 nm), as previously reported[35] and the corresponding images were obtained within the red channel. The resulting images were then merged and the co-localization of the nanocrystals with the lipidic shell evaluated by NIS software.[35,36]

DLS and Z-potential were also performed on the LNCs samples. Furthermore, nanoparticle tracking analysis (NTA) was exploited for an additional evaluation of the nanoconstructs hydrodynamic size distribution and concentration, using a NanoSight NS300 (Malvern Panalytical). The detection was carried out by a $\lambda = 505$ nm laser beam and with a 20x magnification objective. Sample dilution was adjusted to feature within the range of 20–80 particles/frame and three videos of 60 s

were captured for each sample, each with an infusion rate of 30 and a camera level between 11 and 15. Videos were analyzed with the NTA 3.2 software, setting the detection threshold to 5.

Transmission electron microscopy was performed with a Talos F200X G2 S(TEM) from Thermo Scientific. The prepared LNCs were diluted to a concentration of 10 μg mL^{-1} in bidistilled and 0.1 μm microfiltered water and then spotted on a copper holey carbon grid, let dry, and imaged without staining at an operating voltage of 60 kV.

2.6. Drug Release Experiments from Lipid-Coated Nanocrystals

Drug release experiments were performed in complete cell culture medium to i) suggest a release kinetics profile, ii) assess an eventual retention of the drugs previously adsorbed on the NCs surface from the LNCs, and iii) compare LNCs to the lipid-uncoated NCs. All drug delivery experiments were monitored for 96 h, collecting the drug absorbance of the cell culture medium by UV–vis spectroscopy at different time points and referring them to the calibration curves of each drug in. To prepare the calibration curves in RPMI, both stock solutions of Sorafenib (5 mM in ethanol) and of Vismodegib (10 mM in DMSO) were diluted in RPMI at different concentrations (0.001, 0.01, 0.1, 1, 10, 100, 125, 250, and 500 μM) and analyzed in triplicate using a synthetic quartz glass microplate (96 wells, Hellma Analytics).

The following samples were evaluated: Single drug (either Sorafenib or Vismodegib) loaded LNCs, single drug loaded NCs (without liposomal coating), unloaded LNCs and NCs, both as reference. All samples were prepared as pellets of 350 μg by centrifugation, and then resuspended into 700 μL of RPMI (1:2 weight/volume ratio). This solution was then aliquoted in three identical solutions of 200 μL, each containing 100 μg of NCs, and further 800 μL of fresh RPMI was added to all of them.

In this way, triplicate experiments were carried out for each sample type. As blank control samples, a triplicate of 1 mL of cell culture medium was also analyzed. All sample tubes were orbitally shaken at 200 rpm and 37 °C, the released drug was assessed at different time points (0.5, 2, 24, 48, 72, and 96 h) by centrifuging all samples at 10 000 RCF for 5 min, collecting 3 aliquots of 100 μL of supernatant from each one, and reading the UV–vis absorbance with the quartz glass microplate. Control samples were subjected to the same protocol to standardize the treatment and then used as background subtraction.

Once the reading was completed, the 300 μL of each sample was put back into the corresponding tubes, vigorously mixed, and vortexed again for homogenization, to continue with the cumulative release experiment.

2.7. Proof of Concept: In Vitro Cell Culture Experiments

To preliminarily test the final nanoconstructs and assess their behavior in a first proof-of-concept application, the drug-loaded LNCs were tested on three different cell lines: BxPC-3 (a human pancreatic cancer cell line, CRL-1687 from ATCC), AsPC-1 (a human pancreas adenocarcinoma ascites metastasis cell line, CRL-1682 from ATCC), and HPDE (healthy human pancreatic duct epithelial cells, H6c7, CVCL_0P38, from Kerafast).

Cellular uptake of 10 μg mL^{-1} LNCs (without uploaded drugs) were assessed after 20 h of incubation at 37 °C, 5% CO_2 into the pancreatic cancer cells (i.e., AsPC-1 and BxPC-3). Briefly, cells were seeded (5000 cells per well in the above-mentioned cell culture medium) in 8-well chamber slides (Nunc Lab-Tek II CC2 Chamber Slide System, Thermo Fisher Scientific) for live-cell imaging optical fluorescence microscopy 24 h before the assay. The lipidic shell of LNCs was previously labelled by means of the FITC bound to the targeting peptide, while cell membranes with Wheat Germ Agglutinin, Alexa FluorTM 647 Conjugate (WGA647, Thermo Fisher, excitation peak at 650 nm, emission peak at 668 nm).[35]

The cytotoxicity of the drug-loaded LNCs and, as a comparison, the unloaded LNCs, the single drug loaded LNCs and the free drugs were assessed with both pancreatic cancer cell lines. Briefly, cells were seeded in replicates (2500 cells in 100 μL per well) in 96-well plates (Greiner Bio-One) for 24 h before the treatment, then cell media was replaced by solutions constituted by RPMI complete medium with increasing concentrations of 10, 20, 30, 40, and 50 μg NCs mL^{-1}. For the free drugs, the amounts corresponding to those adsorbed on the NCs counterpart were evaluated, diluted in RPMI complete medium and administered to cells. After 48 h of treatment, cell viability was assessed with the addition of 10 μL of WST-1 (CELLPRO-RO Roche) per well, measuring the formazan absorbance at 450 nm with the Multiskan Go microplate spectrophotometer (Thermo Fisher Scientific), using a 620-nm reference after 2 h incubation at standard conditions. Cytotoxicity tests were carried out at least in triplicates. The absorbance values of the cells with the different treatments were normalized to those of the untreated cells and multiplied by 100 to get their percentage of viability, expressed as mean ± standard deviation (SD).

The therapeutic effects of both single and dual drug loaded LNCs were then assessed not only on the cancer cell lines (AsPC-1 and BxPC-3), but also on a healthy pancreatic cell line, HPDE. AsPC-1 and BxPC-3 cell lines were also pre-treated with a conventional chemotherapeutic drug, Gemcitabine, for 24 h at a 10 μM concentration, to simulate the behavior of the cell populations after a first line PDAC treatment. The selected concentration was established according to a previous literature study by Awasthi et al.[40]

In detail, cells were seeded (800 000 cells for BxPC-3 and 1 000 000 for AsPC-1) in T-25 cell culture flasks (CELLSTAR, Greiner, 690160-TRI, sterile) and incubated for 24 h with 5 mL of RPMI complete medium containing 10 μM Gemcitabine. Afterward, their viability was assessed by both an optical microscopy analysis and the trypan blue (Trypan Blue Dye, 0.40% solution, Bio-Rad Laboratories) viability assay, and only the alive cells were considered for further treatments since the dead ones were discarded. Afterward, cells with and without Gemcitabine pre-treatment were seeded, as explained above, in a 96-well plate for 24 h before the treatment with single, dual-drug loaded LNCs and the corresponding free drugs. Here, the LNCs at the concentration of 20 μg mL^{-1} were used (the choice of this concentration will be motivated in Section 3) and incubated with cells for further 48 h prior to assessing the cytotoxicity

with WST-1. Cells without Gemcitabine pre-treatment were used as control.

The evaluation of the apoptosis processes involved in cell death was assessed by flow cytometry analysis (Guava EasyCyte 6-2L, Merck). Cells were seeded (30 000 cells per well) in 24-well plates (Greiner Bio-One), then single and dual drug-loaded LNCs were administered at a concentration of 20 μg mL^{-1}. As control experiments, the same amount of drug adsorbed on the NCs surface was administered as free drugs in RPMI. After 24 h, cells were trypsinized and washed with PBS, and then exposed to a specific reagent kit containing Annexin V and 7-AAD (Guava Nexin Reagent, Luminex) for 30 min. A brief explanation of the kit's mechanism of action can be found in Supporting Information. This reagent kit was also employed to assess the apoptosis processes taking place in cells pre-treated for 24 h with Gemcitabine and then incubated for further 24 h with dual-drug loaded LNCs and with free drugs. The same procedure was carried out with both pancreatic cancer cell lines, as reported above.

2.8. Statistical Analysis

The statistical comparison between the treatment groups was performed using one-way or two-way analysis of variance with Origin software. $***p < 0.001$ and $*p < 0.05$ were considered significant. Independent experiments were performed three-times.

3. Results and Discussions

3.1. Nanocrystals Characterization

FESEM in **Figure 3**a shows the spherical-shaped morphology of the Gd-doped ZnO NCs, with average diameters ranging from 5 to 8 nm. In particular, the histogram in Figure 3b reports the size distribution of a sample of NCs measured from the FESEM image, with a mean diameter of ≈7 nm. These results were comparable to those previously described.[33] The content of Gd dopant was estimated by EDS, confirming a doping level of 1.81 atomic%, in line with our previous results.[33]

Figure 3c reports the XRD pattern of the NCs, showing the high crystallinity of the material in the wurtzite crystalline phase (see also Table S1, Supporting Information) and the absence of unwanted secondary phases.

The hydrodynamic size distribution of the nanocrystals was evaluated by DLS measurements in two different dispersants, EtOH and water (Figure 3d), and Z-potential measurements in water were also performed (Figure S1, Supporting Information). The samples show a narrow size distribution, ranging between 182 and 191 nm (as % number) in EtOH and water, respectively. These distributions are confirmed by the small values of the polydispersity index (PDI) obtained (all lower than 0.2, characteristic of monodispersed samples). The stability of the nanocrystals in water solution was also confirmed by the relatively high value of Z-potential measured in water (Figure S1, Supporting Information).

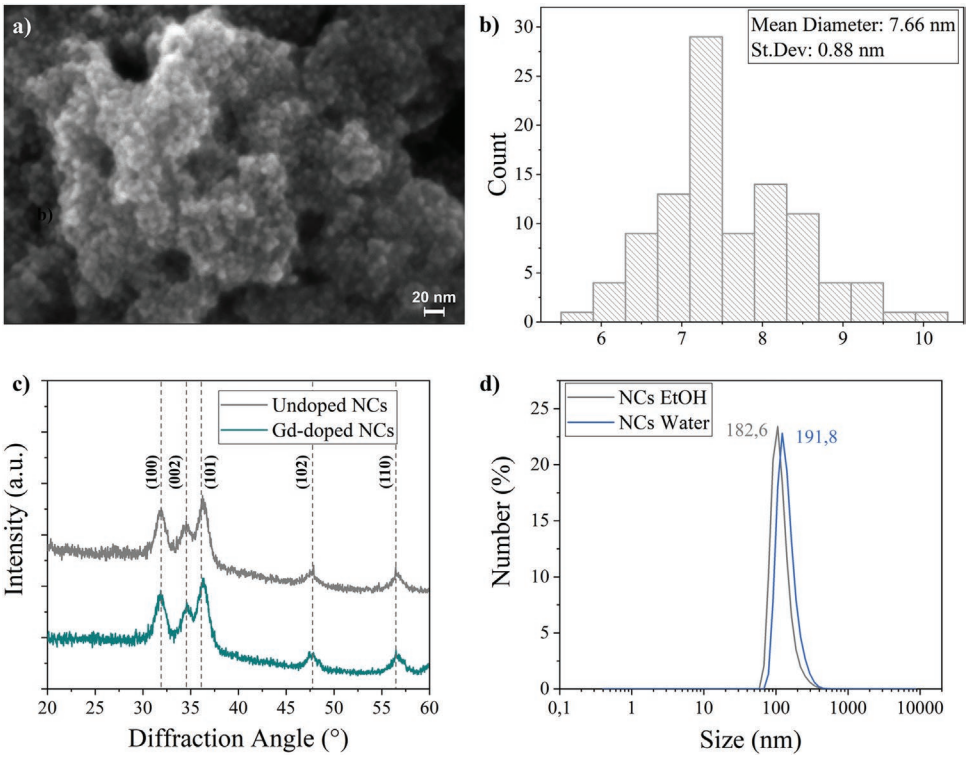

Figure 3. a) FESEM image of amine-functionalized, oleic acid capped Gd-doped ZnO NCs. b) Histogram reporting the dimensions of the Gd-doped ZnO NCs, measured from the FESEM picture. c) XRD diffractograms of undoped and Gd-doped ZnO NCs. d) DLS size distribution of the Gd-doped ZnO NCs in EtOH (grey line) and water (blue line).

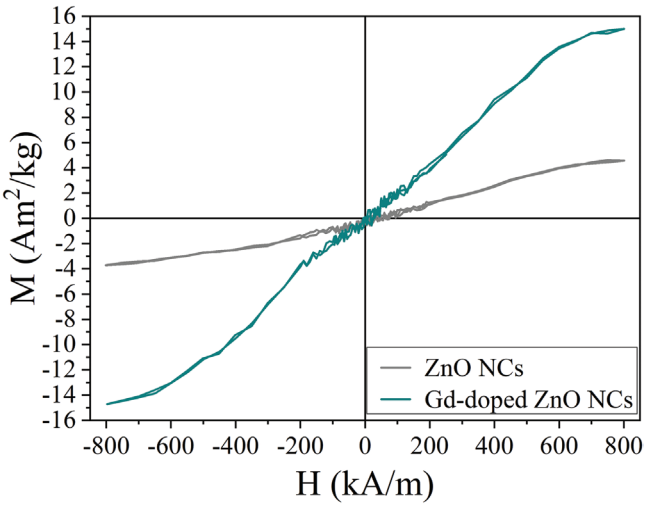

Figure 4. Magnetization-saturation (M-H) curves of oleic acid capped, amino propyl functionalized ZnO NCs and Gd-doped ZnO NCs measured at RT.

It is worth to mention that the higher values of hydrodynamic diameters obtained above with respect to those described by FESEM measurements are due to the method of analysis: dried nanoparticles are indeed considered on FESEM analysis, while hydrated nanomaterials in a liquid solvent, where ions also adsorb on the sample surface thus increasing its steric hindrance, are present in the DLS measurement.

More detailed characterizations, such as HRTEM and XPS were previously reported by us in another work.[33]

The prepared NCs were also characterized in terms of magnetic behavior, as explained above. More in detail, the magnetization in quasistatic conditions was evaluated at RT for the pristine and the Gd-doped ZnO NCs, both functionalized with amino-propyl groups. The results, reported in **Figure 4**, show a paramagnetic behavior for both types of NCs; however, the maximum magnetization obtained with Gd-doped NCs is higher than that of pristine ZnO, due to the presence of Gd atoms inside the ZnO lattice. Doping with rare elements has been already established in the literature as a way to impart magnetic properties to ZnO NCs.[32] The magnetization enhancement, already assessed in Gd-doped ZnO NCs in absence of amino-propyl functionalization in a previous work,[33] is hereby confirmed in the case of functionalized NCs as well. Even if the true motivation of such phenomenon is still under debate, most of the existing literature attributes this enhancement to either the presence of oxides nano-phases inside the ZnO lattice or the introduction of new magnetic dipoles into the NCs.[41] Since, as reported above, the XRD patterns displayed in Figure 3c do not show the presence of any secondary phase apart from the ZnO wurtzite one, it is fair to suppose that the reason of such enhanced magnetization might be due to the introduction of Gd magnetic dipoles into the NCs. Judging from the imaging potentialities of the final nanoconstruct, it is clear that this enhanced magnetization could be explored in order to employ the final nanodevice as a contrast agent for MRI.

3.2. Dual Drug Uptake

Figure 3 reports the preliminary studies performed to optimize the drug uptake time, specifically of Vismodegib in DMSO (**Figure 5**a) and Sorafenib in ethanol (Figure 5b). A similarly high drug adsorption on ZnO NCs was observed for both drugs after the first 2 h. In the case of Vismodegib, the adsorption further increased, reaching a maximum after 3.5–4 h, and then a drug desorption was detected after 6 h of uptake. The uptake of Sorafenib did not improve significantly after the first 2 h, and a decrease was recorded after 6 h. From these trends, the achievement of an equilibrium between adsorption and desorption can be hypothesized for both drugs after a certain time, which can be then responsible for the partial release of the drugs back to their solvent. This is indeed expected in view of the weak bonds (typically hydrogen bonding or van der Waals forces) taking place between both drug molecules and the ZnO NCs surface, decorated with both amine groups and oleic acid.

Some preliminary studies were carried out to assess the best adsorption order of the drugs combination and are reported in detail in Figures S2 and S3, Supporting Information. Putting together the results of these experiments and the above mentioned studies of the single drugs' behavior in their solvents, the optimal time and procedure for the uptake protocol was established: 3.5 h of uptake for Vismodegib in DMSO followed by 2 h of Sorafenib uptake in EtOH. The final uptaken drugs were then evaluated with UV–vis spectroscopy as described above and are reported in Figure 5c.

3.3. Lipid-Coated Nanocrystals Preparation

The NCs were coated with a lipidic bilayer derived from two different liposome formulations, Lipo and Lipo-Pep, to generate the final nanoconstructs (LNCs). Lipo and Lipo-Pep were also first characterized prior to their coupling with NCs, through NTA measurements and Z-potential analyses (see Figure S4, Supporting Information). They exhibited optimal stability and narrow size distribution in water, with average values of 138 nm for Lipo and 147 nm for Lipo-Pep, and a distinct strong negative Z-potential, which can explain in terms of charge repulsion the good dispersity in water.

The NTA results of the LNCs (blue curve in **Figure 6**a) show a narrow size distribution, centered at 105 nm, similar to the freeze-thawed liposomes prepared without NCs as a control (indicated as Lipo-Lipo-Pep in Figure 6, purple curve in Figure 6a). In contrast, the pristine NCs without lipidic coating seem to aggregate, with a size distribution having a major peak at 204 nm (green curve in Figure 6a).

Furthermore, as displayed by Figure 6b, the naked NCs display a Z-potential of +27.8 mV, whereas a negative value is shown for LNCs (−20.8 mV), close to the Z-potential value of −30.4 mV obtained for freeze-thaw control Lipo-Lipo-Pep without NCs.

The TEM imaging (Figure 6c and related image inset) conducted on the LNCs shows groups of NCs (dark dots) encapsulated by round shaped and vanishing organic matter (dark grey) having an overall size of about 100 nm each. It is worth to mention that, despite the LNCs are not stained, the lipidic fraction

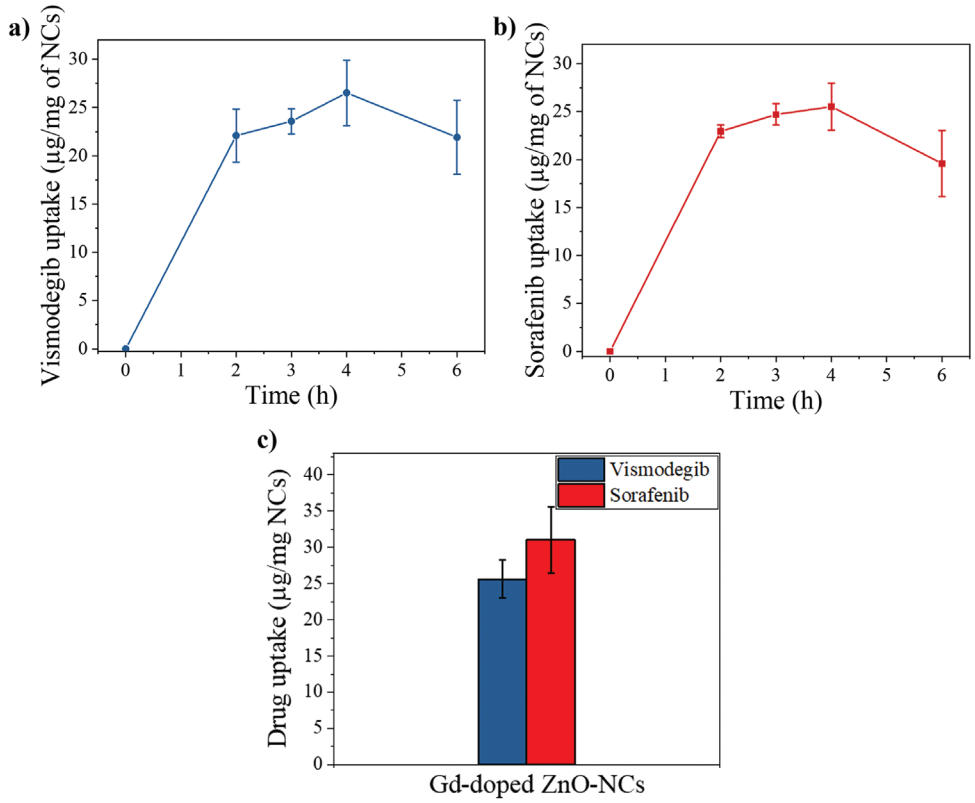

Figure 5. a) Vismodegib uptake in DMSO and b) Sorafenib uptake in ethanol expressed in µg of drug per mg of functionalized Gd-doped ZnO NCs, as a function of time. c) Dual drug uptake at the optimized time point for each drug in their respective solvent expressed in µg of drug per mg of functionalized Gd-doped ZnO NCs.

is still quite visible at the operating voltage used here (60 kV), although rapidly degrading, and allows to argue the incorporation of the nanocrystal into the liposomal membrane.

As a whole, these results nicely suggest the success of the NCs encapsulation process by the liposome using the freeze-thaw method, as both the Z-potential and size distribution of the final LNCs nanoconstruct were similar to the reference liposomes, while TEM images enables a first visualization of the LNCs nanoconstruct.

To further confirm the above-mentioned results, the fluorescence microscopy technique was exploited for a qualitative co-localization study. The NCs were labelled with the Atto550-NHS ester dye and imaged in the red channel, whereas the CKAAKN peptide, linked to the functional lipid and thus conjugated to the liposomal shell, was bound to the FITC dye and visualized in the green channel. Microscope images, reported in **Figure 7**, demonstrate excellent levels of co-localization of the two dyes in the LNCs sample after the freeze-thaw cycles. The co-localization percentage was in fact found to be equal to 92% when a sample of 10 different pictures was analyzed with the co-localization tool of the NIS-element software.

To obtain the final nanoconstruct, dual drug loading (Vismodegib first and then Sorafenib) was performed on the NCs as described above, and then the lipid bilayer was coupled by 6 freeze-thaw cycles to obtain the dual drug loaded LNCs. A rapid characterization of the nanoconstructs was then carried out, compared to the unloaded LNCs.

DLS and Z-potential, reported in **Figure 8**, show very similar size distributions and Z-potential values, suggesting that the presence of both drugs did not change the hydrodynamic properties of the LNCs nor their surface charge.

These results confirmed those obtained in the course of preliminary DLS measurements which aimed at comparing the behavior of drug-loaded NCs and LNCs with respect to unloaded samples. As reported in **Figure 9**, a marked difference can be noticed between NCs and LNCs when loaded with either one or both drugs: while the pristine nanocrystals show a significant increase in their hydrodynamic size and a broader size distribution, probably due to the steric hindrance of the drug molecules (Figure 9a,c,e), the lipid-coated ones do not show any significant alteration when loaded with drugs (Figure 9b,d,f). This behavior might be attributed to the shielding effect of the lipidic coating, which provides the nanoconstructs with colloidal stability thus reducing their aggregation in water, as demonstrated by their narrow size distributions even in the presence of the drugs.

3.4. Single Drug Release in a Cellular Condition

The nanoconstructs loaded with either Sorafenib or Vismodegib were immersed in cell culture medium under continuous stirring at 37 °C with the aims of i) checking the good

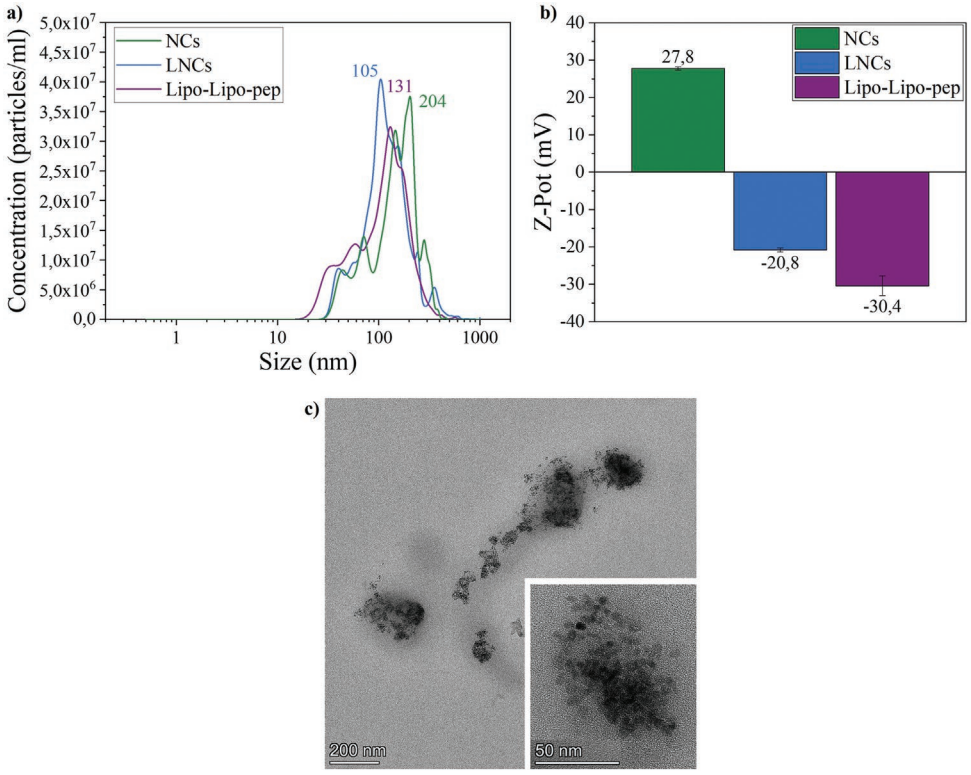

Figure 6. a) NTA and b) Z-potential values of the LNCs nanoconstruct with respect to the control Lipo-Lipo-Pep formulation (with no NCs encapsulated) and the pristine NCs. c) TEM images at 60 kV of the LNCs freshly prepared without any staining.

retention of the drugs at the surface of the ZnO NCs, ii) proving the shielding effect of the lipid coating of the LNCs, and iii) assessing the release profile over time.

The NCs without lipid coating show a more pronounced drug release in comparison with their LNCs counterparts, as reported in **Figure 10**. In fact, the Sorafenib release profile

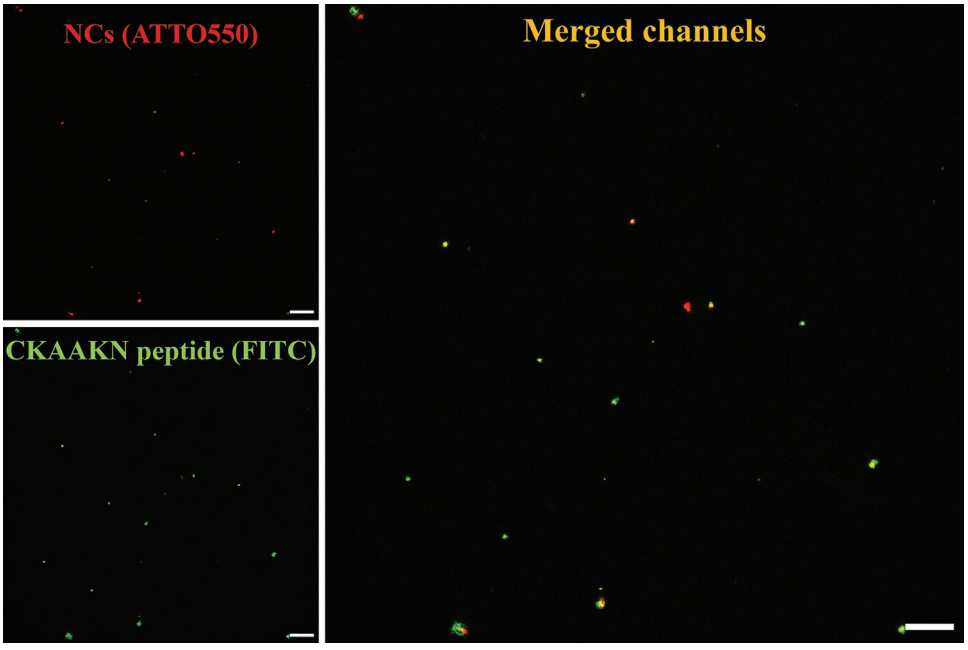

Figure 7. Fluorescence microscopy images of the LNCs nanoconstruct without drugs. Red channel showing the NCs labeled with ATTO550, green channel reporting the FITC dye attached to the CKAAKN peptide and conjugated to the lipid shell and merged channel to appreciate the co-localization. Scale bars are set to 10 µm.

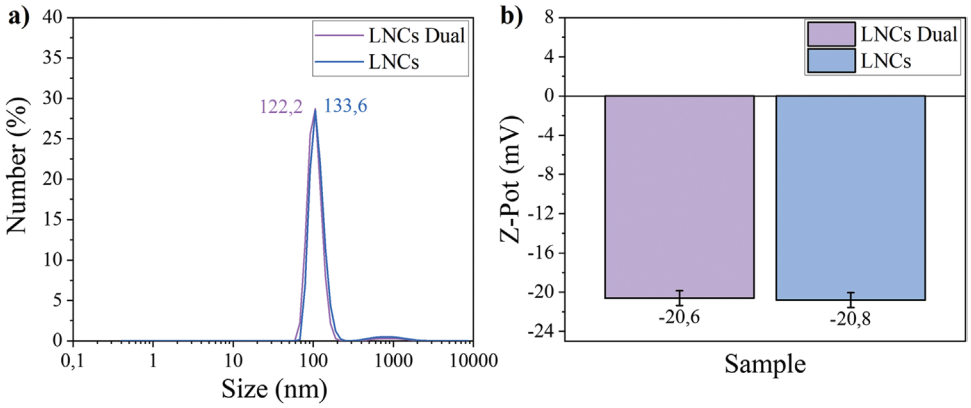

Figure 8. a) DLS size distribution and b) Z-potential measurements of unloaded and dual-drug loaded LNCs.

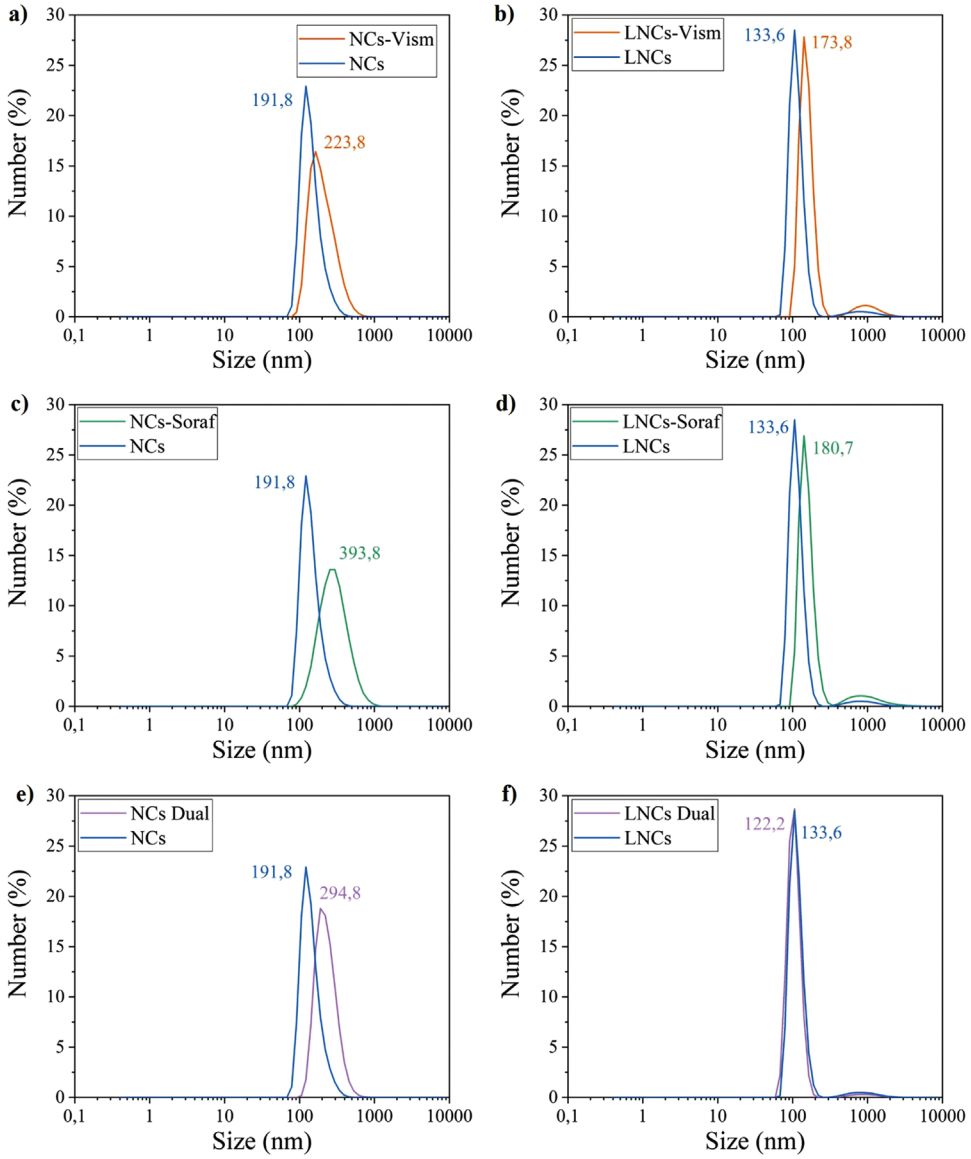

Figure 9. Comparison between NCs and LCs loaded with a,b) Vismodegib, c,d) Sorafenib, and e,f) both drugs, respectively.

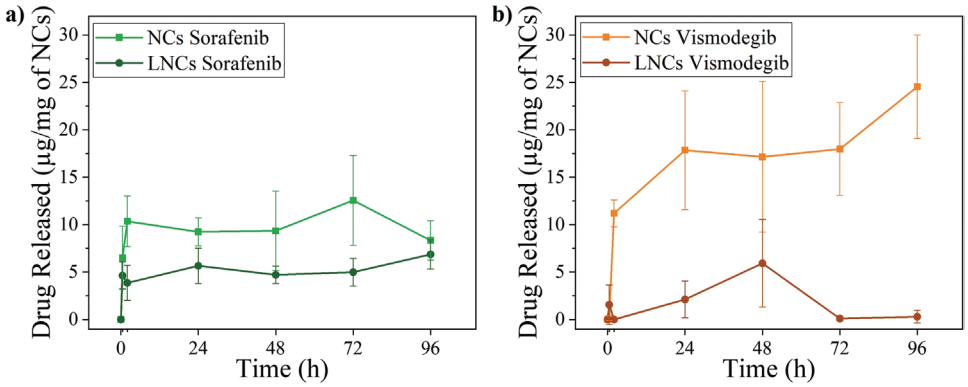

Figure 10. Drug release profile up to 96 h of a) Sorafenib and b) Vismodegib in RPMI at 37 °C comparing the LNCs carriers with the pristine NCs ones.

demonstrates a reduced but sustained release over time from the LNCs (Figure 10a) while the Vismodegib release kinetics from LNCs shows a slowly increasing delivery in the first 48 h, still lower in comparison with the NCs alone (Figure 10b). This behavior is hypothesized to be optimal for future applications, as the rapid initial release of Vismodegib out of the nanoconstruct could be useful for the depletion of tumor stroma in vivo (by inhibiting HH signaling pathway) whereas the moderate but sustained release of Sorafenib over time, having anti-angiogenic effect, is necessary to maintain long-lasting therapeutic conditions in the tumor microenvironment.

Therefore, the lipid bilayer coating seems to act as a shield against the rapid and uncontrolled drug release. These results, combined with the good colloidal stability of LNCs in solution, confirm that the developed nanoconstructs have improved performances in comparison with the NCs alone and can be exploited for in vitro experiments.

Figure S5, Supporting Information, reports the same experiment, this time expressing the release in terms of percentage of the drugs originally uploaded on the nanoconstructs. Figure S6, Supporting Information, instead reports the UV–vis absorption spectra of both drugs in RPMI at 37 °C, used to derive the calibration curves in cell culture media.

3.5. Live-Cell Fluorescence Imaging with Lipid-Coated Nanocrystals

The targeting capability of the CKAAKN peptide toward the two cancer cell lines was preliminarily proofed on Lipo constructs, prior to test the LNCs. Indeed, the analysis performed with flow cytometry in a previous work[38] had already shown the enhanced capability of the CKAAKN peptide. Here, using different mole percentages with respect to the lipidic shell, we also prove to provide an efficient cell internalization (or at least a cell surface binding) to both cell lines (see Figure S7a, Supporting Information).

Therefore, to qualitatively evaluate the internalization level of the LNCs into the BxPC-3 and AsPC-1 cell lines, fluorescence microscopy analyses were performed employing unloaded LNCs.

Figure 11 reports the results obtained on AsPC-1 and BxPC-3 cells. When analyzing the merged channel (panels on the right), a complete internalization of the LNCs, even at a concentration of 10 μg mL^{-1}, can be appreciated, as essentially all green signals (FITC dye bound to the targeting peptide) are located inside the cells. Control experiments on untreated cells imaged in the same channels, evidencing the absence any relevant green background, were also collected (Figure S7b,c, Supporting Information)

3.6. Preliminary Therapeutic Treatments In Vitro

The drug loaded LNCs were tested on BxPC-3 and AsPC-1 cells to assess their therapeutic effects. In particular, cells were treated with single and dual drug loaded LNCs and, as a comparison, with free drugs both as single and as dual drug administrations, using the amount of drug corresponding to that adsorbed on the LNCs.

Figure 12 reports the percentage of viable cells after 48 h of incubation with different concentrations of LNCs and Sorafenib-loaded LNCs, as well as with free Sorafenib drug. The aim of this experiment was to find the cytotoxic threshold and then select the optimal LNCs concentration to be used in the following synergy experiments.

As displayed in Figure 12, both AsPC-1 and BxPC-3 cell lines remained viable upon treatment with the Sorafenib-loaded LNCs and the corresponding free drug up to a NCs concentration of 20 μg mL^{-1}. In contrast, both cell lines showed a prompt reduction (down to 20% or more) of their viability when using Sorafenib-loaded LNCs at concentrations of 30 and 40 μg mL^{-1} (statistical significance $***p < 0.001$ for both cell lines at both concentrations). For each assay, it can be observed that neither the presence of the pristine LNCs, nor that of the Sorafenib as a free drug affected the cell viability, which remained above 90%. More in detail, the unloaded LNCs showed no cytotoxic effects up to values of 30 μg mL^{-1} of concentration, thus proving their good biocompatibility due to the presence of the lipidic shell. This lipid shielding effect had already been proved in previous cytotoxicity studies on AsPC-1 and BxPC-3 cells comparing the effects of NCs and LNCs, whose results are reported in Figure S8, Supporting Information. A negligible cytotoxic behavior can be observed when carrying out the free drug treatment at all experimented concentrations. Therefore, Sorafenib-loaded LNCs were demonstrated to cause significant toxicity ($***p < 0.001$)

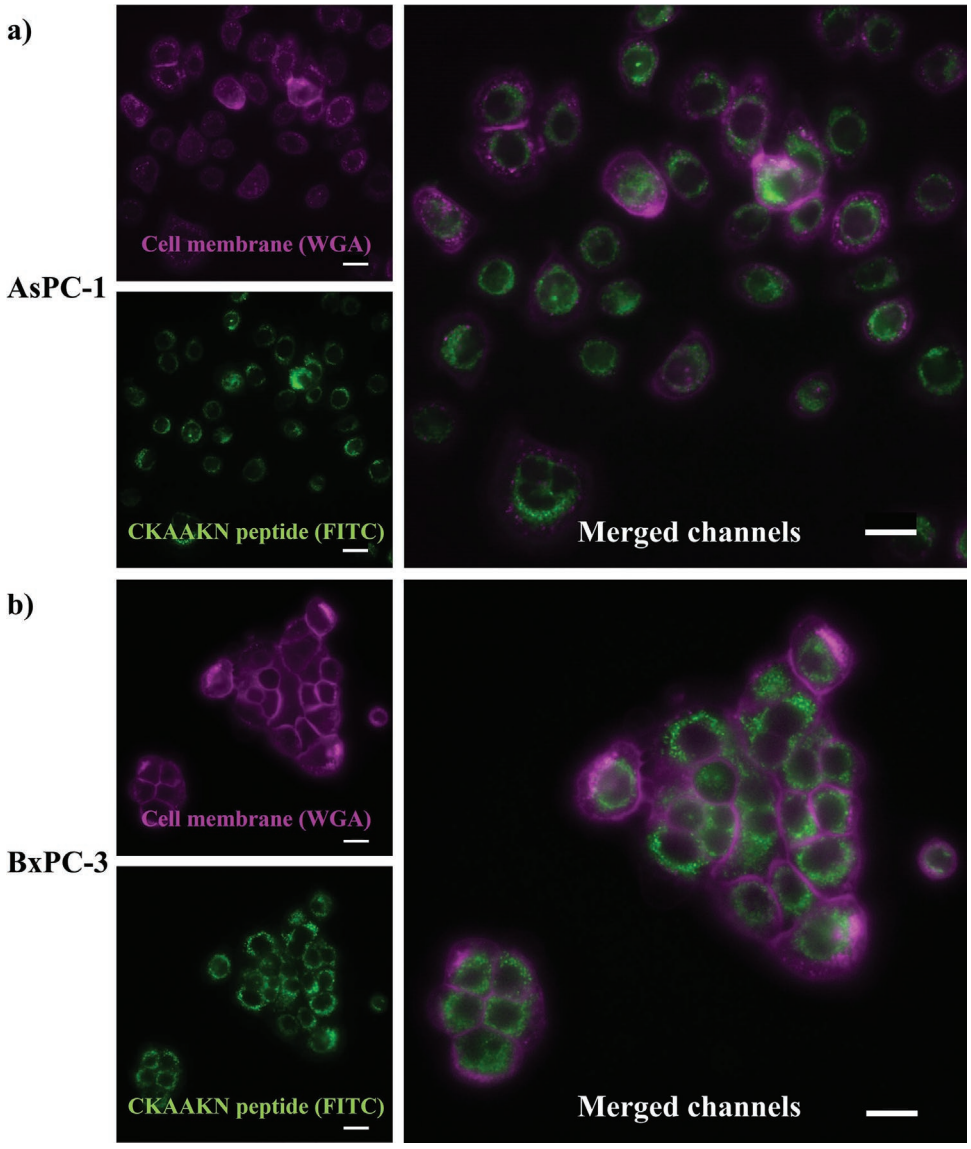

Figure 11. Live cell imaging of LNCs at a concentration of 10 μg mL^{-1} after 20 h of incubation within the pancreatic cancer cells a) AsPC-1 and b) BxPC-3. The cell membranes are labelled with Wheat Germ Agglutinin, Alexa Fluor 647 Conjugate (WGA647) and imaged in the far-red channel (top left panels), while the LNCs are imaged through the FITC dye bound to the peptide and conjugated to the liposomal shell, (green channel, bottom left panels). The merged channels are then visualized, showing the internalization of the LNCs into both cancer cells (right panels). Scale bars are 20 μm.

above a certain threshold with respect to the free drug, remarking the improved efficacy of the treatment when encapsulating the drug-loaded NCs with lipid shell.

Considering the above results in Figure 12, the concentration of LNC-sorafenib (red bar) at 20 μg mL^{-1} seemed the optimal one to be used in the following in vitro experiments to evaluate the effect of the combined drug therapy.

Thus, the cytotoxicity study in **Figure 13** is set at 20 μg mL^{-1} as LNCs concentration. A slight but increased therapeutic efficacy in both AsPC-1 and BxPC-3 cell lines is reported once using the dual-drug loaded LNCs nanoconstructs (grey bars) with respect to the single-drug loaded LNCs (red and blue bars).

A quite remarkable therapeutic efficacy on both cell lines was observed when pre-treating them with Gemcitabine. In detail, a reduction of cell viability of ≈20% was assessed in both Gemcitabine-pretreated (Gem-pretreated) cell lines with the dual drug loaded LNCs (grey bars on the right) with respect to the same case in non-pretreated cancer cells (***$p < 0.001$ for AsPC-1 and *$p < 0.05$ for BxPC-3). Single drug-loaded LNCs (blue and red bars) have a slight reduction in cell viability (less than 10%) in both Gem-pretreated cell lines with respect to the non-pretreated counterpart.

These data thus allow us to hypothesize a synergistic effect of the dual drug loaded combination and its enhanced effectiveness in case of Gem-pretreated cells.

As a control, the corresponding amounts of uploaded drugs were administered as free drug (either single or dual) in RPMI to all cell lines and to pre-treated AsPC-1 and BxPC-3 cells as well. The results, displayed in the patterned bars of Figure 13, did not prove an enhanced cytotoxicity of the free drugs, and

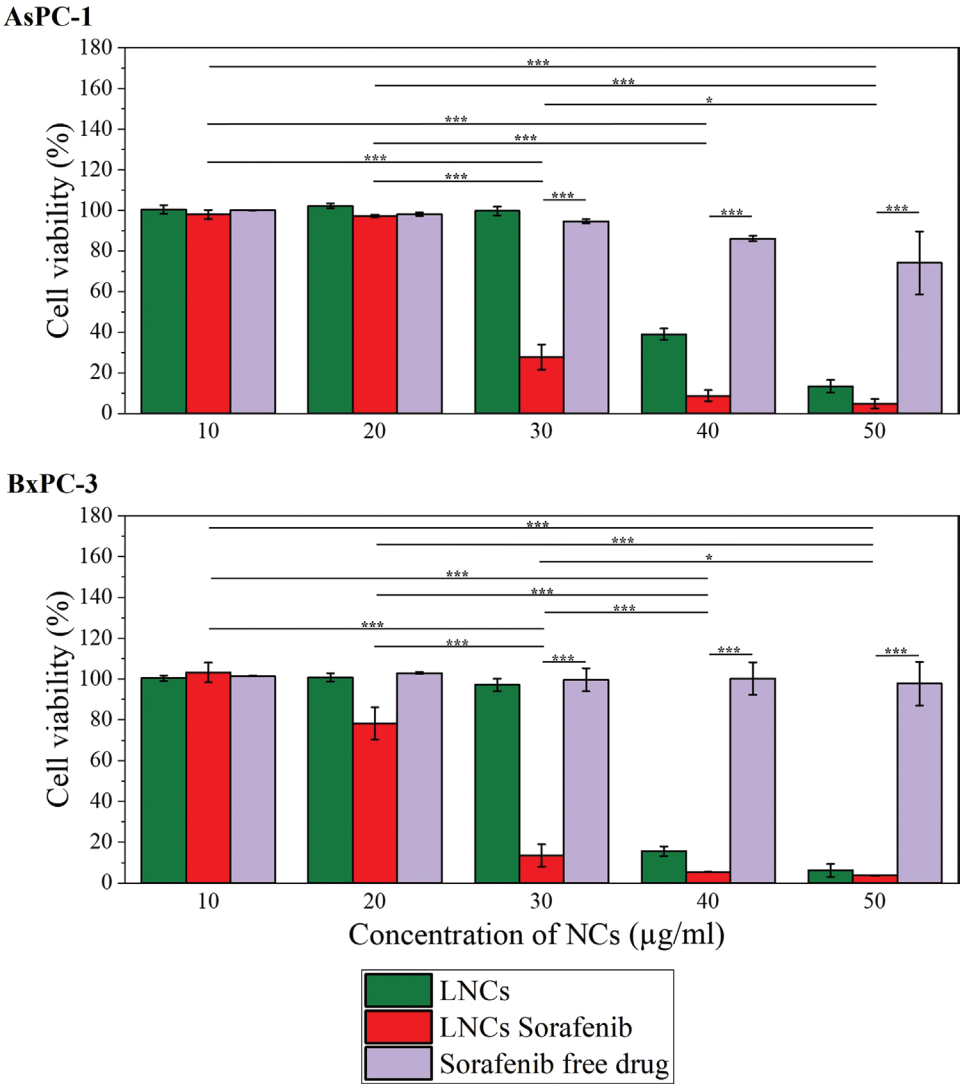

Figure 12. Cell viability assay after 48 h obtained by WST-1 assay for AsPC-1 and BxPC-3 cells. Results are expressed as percentage of cell viability with respect to untreated cells (i.e., 0 μg of NCs mL^{-1}, 100% viability). The comparisons between the different treatments and concentrations were performed using two-way ANOVA; ***$p < 0.001$ and *$p < 0.05$.

thus further corroborated the importance of a conveyed delivery through the nanoconstruct to achieve an increased cell death.

Finally, the results obtained with the healthy HPDE cell line (Figure 13c) show that the cell viability is not compromised by the use of the dual drug loaded LNCs and, as a comparison, by the single drug loaded LNCs and the free drugs. This can be considered as a good preliminary result, since the administration of the LNCs is shown to allow the killing of only cancerous and metastatic cell lines, not influencing the vitality of healthy pancreatic duct cells. With HPDE cells, no statistical significance was reported among the different samples, emphasizing the absence of toxicity toward healthy cells regardless of the presence of the nanocarriers.

3.7. Apoptosis Assays

The first experimental setup of the apoptosis assay regarded a direct treatment of the cells with either drug-loaded LNCs or the equivalent amount of free drug; the second one involved the same cell lines after a 24-h Gemcitabine pre-treatment.

As reported in **Table 1** (and Figures S9 and S10, Supporting Information), the therapeutic effects of the drug-loaded LNCs were significantly higher than that of the free drug counterparts. Actually, the percentages of both the early-apoptotic events and especially the necrosis/late apoptosis ones are larger. However, for BxPC-3 cells, no remarkable differences can be observed in terms of early-apoptotic events occurring after the treatment with drug loaded LNCs with respect to the free drug counterparts.

The above results generally confirm again that, when delivered through the nanoconstruct, both drugs showed an enhanced efficacy of their proper mechanism of action, suggesting the apoptosis of the treated cells.[42,43] These results evidenced a considerable potential of the nanoconstructs in enhancing the treatment of pancreatic cancer through a more efficient drug delivery, showing greater effects on BxPC-3 cancer cells than on metastatic AsPC-1 cells.

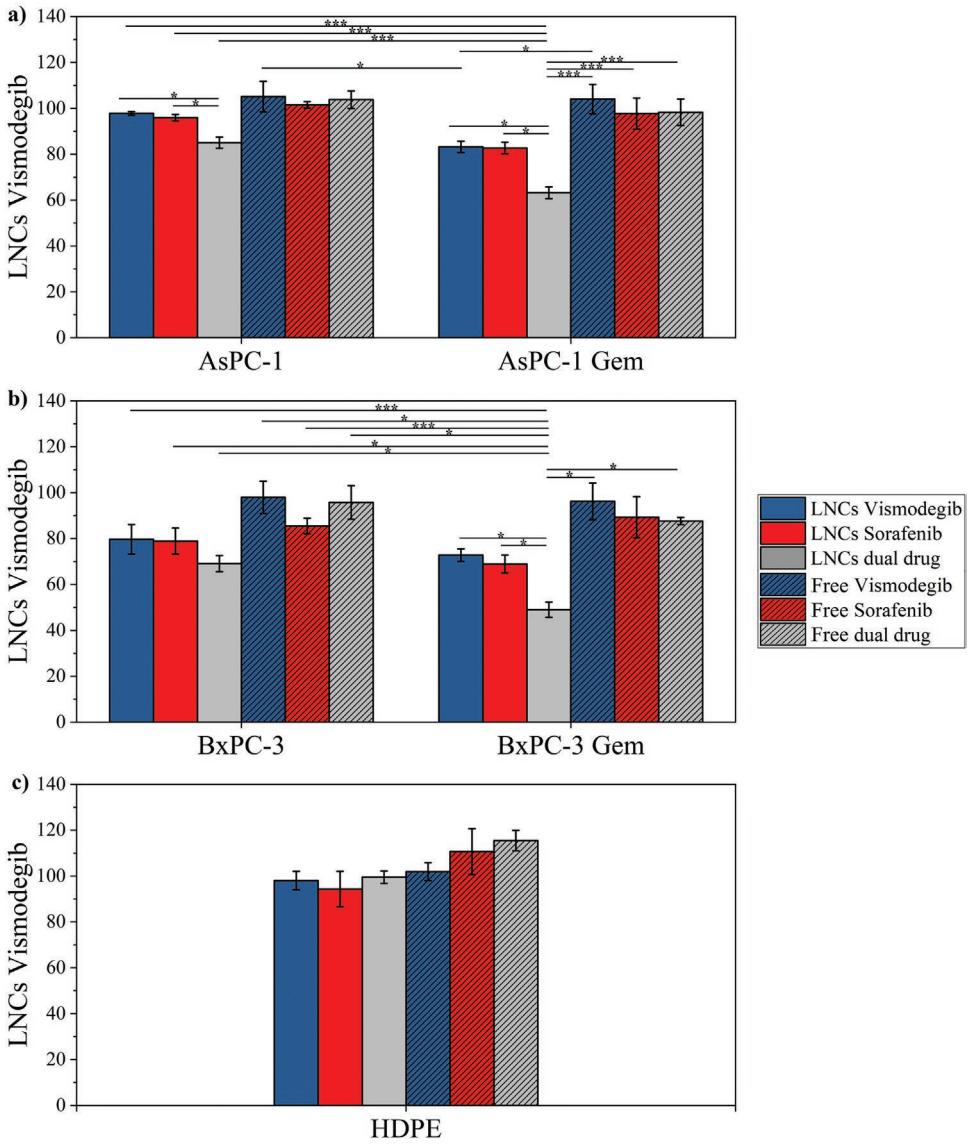

Figure 13. Effect of single and dual drug loaded LNCs (20 μg mL^{-1}) on a) AsPC-1 and b) BxPC-3 cell line, both as such or pre-treated with 10 μM Gemcitabine for 24 h and compared to the free drug administration. c) Effect of single and dual drug loaded LNCs on healthy pancreatic cells (HPDE) after 48 h, compared to the free drugs. Results are expressed as percentage of cell viability with respect to untreated cells (i.e., 0 μg of NCs mL^{-1}, 100% viability). The comparisons between the different treatments and concentrations were performed using two-way ANOVA; ***$p < 0.001$ and *$p < 0.05$.

In the second set of experiments, displayed in **Table 2** (and in Figures S11 and S12, Supporting Information), both AsPC-1 and Bx-PC3 cells show a greater cell death % when tested with dual drug loaded LNC with respect to the control cells or to cell treated with free drug combination. Considering the early-apoptotic events, both cell lines did not show any significant

Table 1. Apoptosis studies under flow cytometry on AsPC-1 and BxPC-3 cells; * = late apoptosis/necrosis.

	AsPC-1 cells		BxPC-3 cells	
	Early apoptosis [%]	Dead cells* [%]	Early apoptosis [%]	Dead cells* [%]
Control cells	2.31	1.15	2.49	3.62
LNCs Sorafenib	3.95	7.80	2.52	11.68
Sorafenib free drug	1.94	1.83	3.73	3.49
LNCs Vismodegib	3.61	6.87	2.26	11.07
Vismodegib free drug	2.26	1.18	3.03	2.65

Table 2. Apoptosis assay on AsPC-1 and BxPC-3 cells pre-treated with Gemcitabine for 24 h and then incubated with either the dual-drug loaded LNCs or the equivalent amounts of free drugs, evaluated 24 h later; * = late apoptosis/necrosis.

		AsPC-1 cells		BxPC-3 cells	
		Early apoptosis [%]	Dead cells* [%]	Early apoptosis [%]	Dead cells* [%]
Not pretreated	Control cells	4.59	4.09	3.18	5.15
	LNCs-dual	5.17	10.13	3.46	11.87
	Free dual	6.62	5.42	4.55	6.11
Gem-pretreated	Control cells	10.62	10.13	8.20	24.30
	LNCs dual	10.98	15.47	5.75	62.11
	Free dual	10.90	11.67	8.46	27.14

difference when treated with dual drug loaded LNCs or free drugs. The same trends can be observed irrespectively to the Gem-pretreated cells or to the non-pretreated one.

Strikingly, the percentage of Gem-pretreated BxPC-3 dead cells is remarkably increased when the dual-drug loaded LNCs are administered to cells with respect to the free drugs. A similar trend is observed for the ASPC-1 cells, but with more moderate increase with respect to the free drug administration.

More modest dead cells percentages were obtained when both ASPC-1 and BxPC-3 cells were not pre-treated with Gemcitabine, while no significant differences were highlighted for the early-apoptotic events in the two different treatment conditions.

Since Gemcitabine's main mode of action has repeatedly been proved to be apoptosis induction in cells,[44,45] it may be assumed that the pre-treated cells which resulted positive to both Annexin V and 7-AAD staining after the administration of the LNCs (dead cells in Tables 1 and 2) could be either the result of a late apoptosis or dead by apoptotic mechanisms. The same hypothesis can be extended to the dual-drug loaded LNCs, since both Vismodegib and Sorafenib have been proven to cause apoptosis when administered to cells derived from other tumors.[42,43] Nevertheless, further studies on the drugs' mechanisms of actions, especially when combined and administered simultaneously to pancreatic cancer cells, will allow a more thorough interpretation of these encouraging preliminary data.

4. Conclusions

The goal of this study was to develop an innovative biomimetic platform based on gadolinium-doped and oleic acid capped zinc oxide nanocrystals with the aim of combining the effect of two inhibitor therapeutic agents, Sorafenib and Vismodegib, whose synergistic in vitro application through a nanoplatform had never been reported so far, to the extent of our knowledge. The results here disclosed are very promising, since these nanocarriers were thoroughly characterized to assess their successful implementation. The core of the nanoconstructs is here reported to meet all the physico-chemical requirements assessed in previous detailed studies; moreover, the incorporation of two different drugs by means of two successive physical adsorptions is an innovative approach that avoids covalent bonds and complex reactions typically involving toxic solvents. The lipidic shell, whose effective coating is demonstrated by the shift in the surface charge of the nanocarriers, is able to both improve the biostability and reduce aggregation in water based media, as shown by numerous size analyses. In addition to that, the incorporation of the CKAAKN targeting peptide into the lipidic shell is a successful and easy way to impart tumor targeting capabilities to the nanoconstruct. As a first step toward in vivo validation, the cytotoxicity studies here presented seem to confirm the synergistic action of the two drugs when administered simultaneously by means of these nanovehicles. In particular, the proved therapeutic effect on cancer cells with respect to the free drugs and their manifest ability to both preserve the drugs' mechanisms of action and spare healthy cells are interesting cues for future works.

Taken together, these findings can be considered an optimal starting point to overcome two of the major drawbacks of traditional chemotherapy, namely the lack of selectivity toward cancer cells and the high toxicity toward healthy tissues resulting from the combination of multiple drugs. This therapeutic outcome can be expected to have a significant impact not only on PDAC treatment, but also for other stroma-rich cancers.

Supporting Information

Supporting Information is available from the Wiley Online Library or from the author.

Acknowledgements

This work received funding from the European Commission under a Marie Skłodowska–Curie Actions grant (Standard European Individual Fellowships, H2020-MSCA-IF-2018, Grant Agreement No. 842964, Project Acronym "MINT") and funding received by Ministero dell'Università e della Ricerca under the Dipartimento di Eccellenza 2018–2022 program.

Open Access Funding provided by Politecnico di Torino within the CRUI-CARE agreement.

Conflict of Interest

The authors declare no conflict of interest.

Author Contributions

S.B. and M.C. contributed equally to this work. Conceptualization—S.B. and V.C.; Methodology—S.B. and L.R.; Software—M.C.;

Validation—S.B., M.C., N.M.P., and R.M.G.M.; Formal analysis—S.B., M.C., and L.R.; Investigation—S.B., M.C., N.M.P., R.M.G.M., and M.A.; Resources—V.C.; Data curation—S.B., M.C., and L.R.; Writing—original draft preparation—M.C. and V.C.; Writing—review and editing—S.B. and L.R.; Supervision—V.C.; Project administration—V.C.; Funding acquisition—S.B. and V.C. All authors have read and agreed to the published version of the manuscript.

Data Availability Statement

The data that support the findings of this study are available in the supplementary material of this article.

Keywords

dual drug delivery, supported lipid bilayer, synergistic nanotheranostics, targeting peptide, zinc oxide nanocrystals

Received: July 26, 2022
Revised: December 12, 2022
Published online:

[1] R. L. Siegel, K. D. Miller, H. E. Fuchs, A. Jemal, *Ca-Cancer J. Clin.* **2021**, *71*, 7.
[2] H. Sung, J. Ferlay, R. L. Siegel, M. Laversanne, I. Soerjomataram, A. Jemal, F. Bray, *Ca-Cancer J. Clin.* **2021**, *71*, 209.
[3] D. von Ahrens, T. D. Bhagat, D. Nagrath, A. Maitra, A. Verma, *J. Hematol. Oncol.* **2017**, *10*, 76.
[4] V. L. Veenstra, A. Garcia-Garijo, H. W. van Laarhoven, M. F. Bijlsma, *Cancers* **2018**, *10*, 34.
[5] A. Cannon, C. Thompson, B. R. Hall, M. Jain, S. Kumar, S. K. Batra, *Genes Cancer* **2018**, *9*, 78.
[6] A. N. Hosein, R. A. Brekken, A. Maitra, *Nat. Rev. Gastroenterol. Hepatol.* **2020**, *17*, 487.
[7] M. Conte, V. Cauda, *Adv. Ther.* **2022**, *5*, 2200079.
[8] D. Gu, K. E. Schlotman, J. Xie, *J. Biomed. Res.* **2016**, *30*, 353.
[9] K. B. Stopa, A. A. Kusiak, M. D. Szopa, P. E. Ferdek, M. A. Jakubowska, *Int. J. Mol. Sci.* **2020**, *21*, 3218.
[10] K. P. Olive, M. A. Jacobetz, C. J. Davidson, A. Gopinathan, D. McIntyre, D. Honess, B. Madhu, M. A. Goldgraben, M. E. Caldwell, D. Allard, K. K. Frese, G. Denicola, C. Feig, C. Combs, S. P. Winter, H. Ireland-Zecchini, S. Reichelt, W. J. Howat, A. Chang, M. Dhara, L. Wang, F. Rückert, R. Grützmann, C. Pilarsky, K. Izeradjene, S. R. Hingorani, P. Huang, S. E. Davies, W. Plunkett, M. Egorin, et al, *Science* **2009**, *324*, 1457.
[11] J. Gu, H. Saiyin, D. Fu, J. Li, *Pancreas* **2018**, *47*, 382.
[12] A. D. Rhim, P. E. Oberstein, D. H. Thomas, E. T. Mirek, C. F. Palermo, S. A. Sastra, E. N. Dekleva, T. Saunders, C. P. Becerra, I. W. Tattersall, C. B. Westphalen, J. Kitajewski, M. G. Fernandez-Barrena, M. E. Fernandez-Zapico, C. Iacobuzio-Donahue, K. P. Olive, B. Z. Stanger, *Cancer Cell* **2014**, *25*, 735.
[13] K. E. Craven, J. Gore, M. Korc, *Cancer Lett.* **2016**, *381*, 201.
[14] T. Annese, R. Tamma, S. Ruggieri, D. Ribatti, *Cancers* **2019**, *11*, 381.
[15] V. Longo, O. Brunetti, A. Gnoni, S. Cascinu, G. Gasparini, V. Lorusso, D. Ribatti, N. Silvestris, *OncoTargets Ther.* **2016**, *7*, 58649.
[16] J. Zhao, H. Wang, C.-H. Hsiao, D. S.-L. Chow, E. J. Koay, Y. Kang, X. Wen, Q. Huang, Y. Ma, J. A. Bankson, S. E. Ullrich, W. Overwijk, A. Maitra, D. Piwnica-Worms, J. B. Fleming, C. Li, *Biomaterials* **2018**, *159*, 215.
[17] R. K. Jain, *J. Clin. Oncol.* **2013**, *31*, 2205.
[18] F. Sabir, M. Zeeshan, U. Laraib, M. Barani, A. Rahdar, M. Cucchiarini, S. Pandey, *Cancers* **2021**, *13*, 3396.
[19] J. Shi, P. W. Kantoff, R. Wooster, O. C. Farokhzad, *Nat. Rev. Cancer* **2017**, *17*, 20.
[20] R. van der Meel, E. Sulheim, Y. Shi, F. Kiessling, W. J. M. Mulder, T. Lammers, *Nat. Nanotechnol.* **2019**, *14*, 1007.
[21] N. Ahmed, H. Fessi, A. Elaissari, *Drug Discovery Today* **2012**, *17*, 928.
[22] F. Chen, E. B. Ehlerding, W. Cai, *J. Nucl. Med.* **2014**, *55*, 1919.
[23] K. H. Bae, H. J. Chung, T. G. Park, *Mol. Cells* **2011**, *31*, 295.
[24] D. Caputo, D. Pozzi, T. Farolfi, R. Passa, R. Coppola, G. Caracciolo, *World J. Gastrointest. Oncol.* **2021**, *13*, 231.
[25] L. R. Jaidev, D. R. Chellappan, D. V. Bhavsar, R. Ranganathan, B. Sivanantham, A. Subramanian, U. Sharma, N. R. Jagannathan, U. M. Krishnan, S. Sethuraman, *Acta Biomater.* **2017**, *49*, 422.
[26] F. Yang, C. Jin, S. Subedi, C. L. Lee, Q. Wang, Y. Jiang, J. Li, Y. Di, D. Fu, *Cancer Treat. Rev.* **2012**, *38*, 566.
[27] S. Campora, G. Ghersi, Preprints 2021, 2021020619, **2021**.
[28] J. A. Roacho-Pérez, E. N. Garza-Treviño, P. Delgado-Gonzalez, Z. G-Buentello, J. L. Delgado-Gallegos, C. Chapa-Gonzalez, M. Sánchez-Domínguez, C. N. Sánchez-Domínguez, J. F. Islas, *Life* **2021**, *11*, 1187.
[29] G. Bisht, S. Rayamajhi, *Nanobiomedicine* **2016**, *3*, 9.
[30] L. Racca, M. Canta, B. Dumontel, A. Ancona, T. Limongi, N. Garino, M. Laurenti, G. Canavese, V. Cauda, in *Smart Nanoparticles for Biomedicine*, (Ed: G. Ciofani), Elsevier, Amsterdam **2018**, pp. 171–187.
[31] N. Garino, T. Limongi, B. Dumontel, M. Canta, L. Racca, M. Laurenti, M. Castellino, A. Casu, A. Falqui, V. Cauda, *Nanomaterials* **2019**, *9*, 212.
[32] M. Carofiglio, S. Barui, V. Cauda, M. Laurenti, *Appl. Sci.* **2020**, *10*, 5194.
[33] S. Barui, R. Gerbaldo, N. Garino, R. Brescia, F. Laviano, V. Cauda, *Nanomaterials* **2020**, *10*, 1150.
[34] A. Luchini, G. Vitiello, *Front. Chem.* **2019**, *7*, 343.
[35] B. Dumontel, M. Canta, H. Engelke, A. Chiodoni, L. Racca, A. Ancona, T. Limongi, G. Canavese, V. Cauda, *J. Mater. Chem. B* **2017**, *5*, 8799.
[36] A. Ancona, B. Dumontel, N. Garino, B. Demarco, D. Chatzitheodoridou, W. Fazzini, H. Engelke, V. Cauda, *Nanomaterials* **2018**, *8*, 143.
[37] B. Dumontel, F. Susa, T. Limongi, M. Canta, L. Racca, A. Chiodoni, N. Garino, G. Chiabotto, M. L. Centomo, Y. Pignochino, V. Cauda, *Nanomed* **2019**, *14*, 2815.
[38] S. Barui, N. M. Percivalle, M. Conte, B. Dumontel, L. Racca, M. Carofiglio, V. Cauda, *Cancer Nano* **2022**, *13*, 37.
[39] S. Valetti, F. Maione, S. Mura, B. Stella, D. Desmaële, M. Noiray, J. Vergnaud, C. Vauthier, L. Cattel, E. Giraudo, P. Couvreur, *J. Controlled Release* **2014**, *192*, 29.
[40] N. Awasthi, C. Zhang, A. M. Schwarz, S. Hinz, C. Wang, N. S. Williams, M. A. Schwarz, R. E. Schwarz, *Carcinogenesis* **2013**, *34*, 2361.
[41] M. Carofiglio, M. Laurenti, V. Vighetto, L. Racca, S. Barui, N. Garino, R. Gerbaldo, F. Laviano, V. Cauda, *Nanomaterials* **2021**, *11*, 2628.
[42] J. Fernando, P. Sancho, C. M. Fernández-Rodriguez, J. L. Lledó, L. Caja, J. S. Campbell, N. Fausto, *J. Cell. Physiol.* **2012**, *227*, 1319.
[43] C. Wu, S. Hu, J. Cheng, G. Wang, K. Tao, *Exp. Ther. Med.* **2017**, *13*, 2529.
[44] P.-H. Jiang, Y. Motoo, N. Sawabu, T. Minamoto, *World J. Gastroenterol.* **2006**, *12*, 1597.
[45] R. Hill, M. Rabb, P. A. Madureira, D. Clements, S. A. Gujar, D. M. Waisman, C. A. Giacomantonio, P. W. K Lee, *Cell Death Dis.* **2013**, *4*, e791.